Calibration artefacts in KAT-7 data

T. L. Grobler[1,2], O. M. Smirnov*[1,2], C.D. Nunhokee[1]

[1] *Department of Physics and Electronics, Rhodes University, PO Box 94, Grahamstown, 6140, South Africa,*

trienkog@gmail.com,osmirnov@gmail.com,ridhima_24@yahoo.com

[2] *SKA South Africa, 3rd Floor, The Park, Park Road, Pinelands, 7405, South Africa*

Abstract

In [2] we focused on explaining the ghost pattern that appears during the calibration of a regular east-west array. This paper will concentrate on extending our previous results to a general irregular array layout. In radio interferometry calibration refers to the estimation and correction of instrumental and environmental errors induced onto interferometric data. Ghosts are point-like spurious artefacts that are created when calibrating interferometric data with an incomplete sky model. For a regular east west array (given a two-source scenario) we found that each baseline produces its own unique ghost pattern and that these ghosts always appeared in a straight line. Moreover, we found that the spacing between the the ghosts produced for each baseline were inversely proportional to baseline length. In this, paper we will show that for a general irregular layout, ghosts no longer form in a straight line.

1 Introduction

It has been known for a long time that naive calibration can lead to detrimental artefacts, which include the suppression and deformation of real emission as well as the generation of spurious emission [3, 4]. The underlying mechanism by which this comes about is however poorly understood. A recent paper [2], has made some progress in understanding the underlying mechanism which leads to calibration artefacts. The scope of [2] is however very limited, since it only deals with a two-source case study and a regular east-west array. In this paper we extend the calibrated visibility results in [2] to a general array layout.

At this point it is also prudent to point out the relevance of studying calibration artefacts. Calibration artefacts are usually quite faint. With the increased sensitivity of modern telescopes on top of shallow calibration pipelines we can no longer afford to ignore them. Intensity mapping, stacking and Epoch of Reionization (EoR) detection techniques purport to recover signal from "below the noise" [2]. It is therefore crucial to understand the structure of our artefacts that are buried "below the noise".

2 Calibration and uv-Coverage

Calibration can be formulated as a minimization problem. Find the antenna gains $\boldsymbol{g}$ that minimizes:

$$||\boldsymbol{\mathcal{R}} - \boldsymbol{G}\boldsymbol{\mathcal{M}}\boldsymbol{G}^H|| = ||\boldsymbol{\mathcal{R}} - \boldsymbol{g}\boldsymbol{g}^H \odot \boldsymbol{\mathcal{M}}|| = ||\boldsymbol{\mathcal{R}} - \boldsymbol{\mathcal{G}} \odot \boldsymbol{\mathcal{M}}||, \tag{1}$$

where $\boldsymbol{\mathcal{R}}$ is the observed unpolarized visibilities matrix, $\boldsymbol{\mathcal{M}}$ is the calibration model matrix, $\boldsymbol{\mathcal{G}} \odot \boldsymbol{\mathcal{M}}$ is the calibrated visibility matrix, $\boldsymbol{g}$ is the antenna gains matrix, $\boldsymbol{G}$ is equal to diag($\boldsymbol{g}$), $\boldsymbol{\mathcal{G}} = \boldsymbol{G}\boldsymbol{1}\boldsymbol{G}^H = \boldsymbol{g}\boldsymbol{g}^H$, "$H$" denotes the Hermitian transpose and "$\odot$" denotes the Hadamard product. The entries of $\boldsymbol{\mathcal{R}}$, $\boldsymbol{\mathcal{M}}$ and $\boldsymbol{\mathcal{G}}$ are respectively denoted by r_{pq}, m_{pq} and g_{pq}.

It is well known that the u_{pq} and v_{pq} components of a single baseline traces out an elliptical locus $\boldsymbol{b}_{pq}(t) = (u_{pq}(t), v_{pq}(t))^T$ in the uv-plane [5]. Moreover, linear transformations can be used to map the elliptical locus onto a circular locus. The following linear transformations play a crucial part in the remaining sections:

$$\hat{X}_{pq}(\boldsymbol{b}) = \phi_{pq}\boldsymbol{D}(\delta_0)\boldsymbol{T}(\theta_{pq})\boldsymbol{b} + \Delta\boldsymbol{b}_{pq}, \tag{2}$$

$$\tilde{X}_{pq}(\boldsymbol{b}) = \phi_{pq}\boldsymbol{D}(\delta_0)\boldsymbol{b} + \Delta\boldsymbol{b}_{pq}, \tag{3}$$

$$X_{pq}(\boldsymbol{b}) = \phi_{pq}\boldsymbol{D}(\delta_0)\boldsymbol{T}(\theta_{pq})\boldsymbol{b}, \tag{4}$$

where $\boldsymbol{b} = (u, v)^T$ is a free parameter, δ_0 is the declination of the field-center and

$$\boldsymbol{D}(\delta_0) = \begin{pmatrix} 1 & 0 \\ 0 & \sin(\delta_0) \end{pmatrix}, \tag{5}$$

$$\boldsymbol{T}(\theta_{pq}) = \begin{pmatrix} \cos(\theta_{pq}) & -\sin(\theta_{pq}) \\ \sin(\theta_{pq}) & \cos(\theta_{pq}) \end{pmatrix}. \tag{6}$$

The remaining quantities (ϕ_{pq}, θ_{pq} and $\Delta\boldsymbol{b}_{pq} = (0, \Delta b_{pq})^T$) are all defined in fig. 1. In fig. 1, $\hat{X}_{pq}^{-1}(\boldsymbol{b})$ denotes the (functional) inverse of $\hat{X}_{pq}(\boldsymbol{b})$.

978-1-4673-5225-3/14/$31.00 ©2014 IEEE

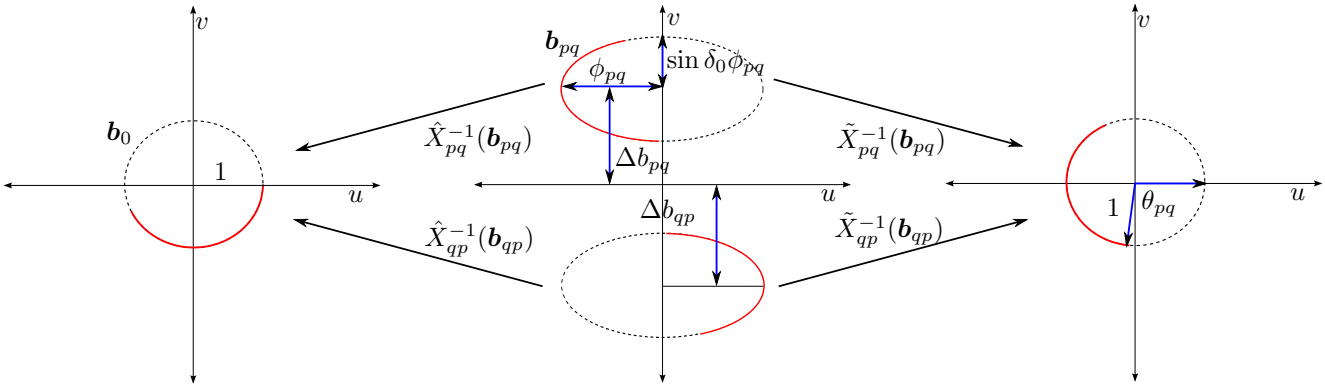

Figure 1: The uv-coverage of a single baseline pq. There exists a linear transformation $\hat{X}_{pq}^{-1}(\boldsymbol{b})$ between the elliptical locus $\boldsymbol{b}_{pq}(t)$ associated with a single baseline and the circular locus $\boldsymbol{b}_0(t)$.

3 Extrapolated visibilities

If you had a perfect interferometer and you were observing a sky that consisted of two unpolarized point sources, one at the field center and another off-center, then your observed visibilities would be completely described by

$$r(\boldsymbol{u}) = A_1 + A_2 e^{2\pi \boldsymbol{u}^T \boldsymbol{s}_0}, \tag{7}$$

where the centre source has flux A_1 and the off-center source has flux A_2, $\boldsymbol{s}_0 = (l_0, m_0)$ is the position vector (in direction cosines) of the off-center source and $\boldsymbol{u} = (u, v)^T$ is a free parameter.

The visibilities that each baseline would observe would then be equal to $r(\boldsymbol{b}_{pq}) = r(\hat{X}_{pq}(\boldsymbol{b}_0))$. The entries of $\boldsymbol{\mathcal{R}}$ are therefore functions of $\boldsymbol{b}_0$, $r_{pq}(\boldsymbol{b}_0) := r(\hat{X}_{pq}(\boldsymbol{b}_0))$. The visibility matrix $\boldsymbol{\mathcal{R}}$ is actually a function-valued matrix $\boldsymbol{\mathcal{R}}(\boldsymbol{b}_0) : \mathbb{R}^2 \to \mathbb{C}^{n\times n}$. We can now define an extrapolated visibility matrix $\boldsymbol{\mathcal{R}}(\boldsymbol{b})$ by replacing $\boldsymbol{b}_0$ by a free parameter $\boldsymbol{b} = (u, v)^T$. Each entry of $\boldsymbol{\mathcal{R}}(\boldsymbol{b})$ is therefore an extrapolated visibility plane which is related to the visibility plane defined in Eq. 7 via the linear transformation $\hat{X}_{pq}(\boldsymbol{b})$. Assuming, that our calibration model only contains the central source, we can solve the extrapolated variant of Eq. 1 via alternating least squares calibration [1]:

$$\boldsymbol{\mathcal{G}}(\boldsymbol{b}) = \lambda(\boldsymbol{b})\mathbf{x}(\boldsymbol{b})\mathbf{x}^H(\boldsymbol{b}), \tag{8}$$

where $\lambda(\boldsymbol{b})$ is the largest eigenvalue of $\boldsymbol{\mathcal{R}}(\boldsymbol{b})$ and $\mathbf{x}(\boldsymbol{b})$ is the unit eigenvector that is associated with $\lambda(\boldsymbol{b})$.

To get $r_{pq}(\boldsymbol{b})$ to equal the visibility plane described in Eq. 7 we have to reverse the effect of $\hat{X}_{pq}(\boldsymbol{b})$, which is accomplished by using the inverse transformation $\hat{X}_{pq}^{-1}(\boldsymbol{b})$. Applying the inverse transformation $\hat{X}_{pq}^{-1}(\boldsymbol{b})$ to $\boldsymbol{\mathcal{R}}(\boldsymbol{b})$ has the following effect on its entries:

$$\boldsymbol{\mathcal{R}}(\hat{X}_{pq}^{-1}(\boldsymbol{b})) \implies r_{pq}(\hat{X}_{pq}^{-1}(\boldsymbol{b})) = r(\hat{X}_{pq} \circ \hat{X}_{pq}^{-1}(\boldsymbol{b})) = r(\boldsymbol{b}) \tag{9}$$

$$\boldsymbol{\mathcal{R}}(\hat{X}_{pq}^{-1}(\boldsymbol{b})) \implies r_{rs}(\hat{X}_{pq}^{-1}(\boldsymbol{b})) = r(\hat{X}_{rs} \circ \hat{X}_{pq}^{-1}(\boldsymbol{b})), \tag{10}$$

where $\circ$ denotes function composition.

Clearly, unwanted frequencies remain in the non-pq funtions. Since $g_{pq}(\hat{X}_{pq}^{-1}(\boldsymbol{b}))$ is dependent on all the elements of $\boldsymbol{\mathcal{R}}(\hat{X}_{pq}^{-1}(\boldsymbol{b}))$ some of the uncanceled frequencies from the remaining baselines (which lead to the strongest ghosts — an approximate ghost map) leak into $g_{pq}(\hat{X}_{pq}^{-1}(\boldsymbol{b}))$ (see Eq. 8). Extending this argument leads to a good approximation of $g_{pq}(\hat{X}_{pq}^{-1}(\boldsymbol{b}))$:

$$g_{pq}(\hat{X}_{pq}^{-1}(\boldsymbol{b})) \approx c_{0,pq} + \sum_{r\neq s} c_{rs,pq} e^{-2\pi i [X_{rs}\circ X_{pq}^{-1}(\boldsymbol{b})]^T \cdot \boldsymbol{s}_0}, \tag{11}$$

where

$$c_{0,pq} = \lim_{\boldsymbol{a}\to\boldsymbol{\infty}} \frac{1}{4a_1a_2} \int_{-\boldsymbol{a}}^{\boldsymbol{a}} g_{pq}(\hat{X}_{pq}^{-1}(\boldsymbol{b}))d\boldsymbol{b}, \tag{12}$$

$$c_{rs,pq} = \lim_{\boldsymbol{a}\to\boldsymbol{\infty}} \frac{1}{4a_1a_2} \int_{-\boldsymbol{a}}^{\boldsymbol{a}} g_{pq}(\hat{X}_{pq}^{-1}(\boldsymbol{b}))e^{2\pi i [X_{rs}\circ X_{pq}^{-1}(\boldsymbol{b})]^T \cdot \boldsymbol{s}_0} d\boldsymbol{b}. \tag{13}$$

The results in this paper were derived from a KAT-7 measurement set at an observational frequency of 1.445 GHz and a field-center declination of $-74.66°$. The baseline of interest was created from antenna 4 and 5 (numbered from 0). The center source is 1 Jy, while the off-center source is 0.2 Jy at $(1°, 0°)$. The functions $r_{4,5}(\hat{X}_{4,5}^{-1}(\boldsymbol{b}))$ and $g_{4,5}(\hat{X}_{4,5}^{-1}(\boldsymbol{b}))$ are depicted in Fig. 2. The functions $r_{4,5}(\hat{X}_{4,5}^{-1}(\boldsymbol{b}_{4,5}))$ and $g_{4,5}(\hat{X}_{4,5}^{-1}(\boldsymbol{b}_{4,5}))$ are depicted in Fig. 3.

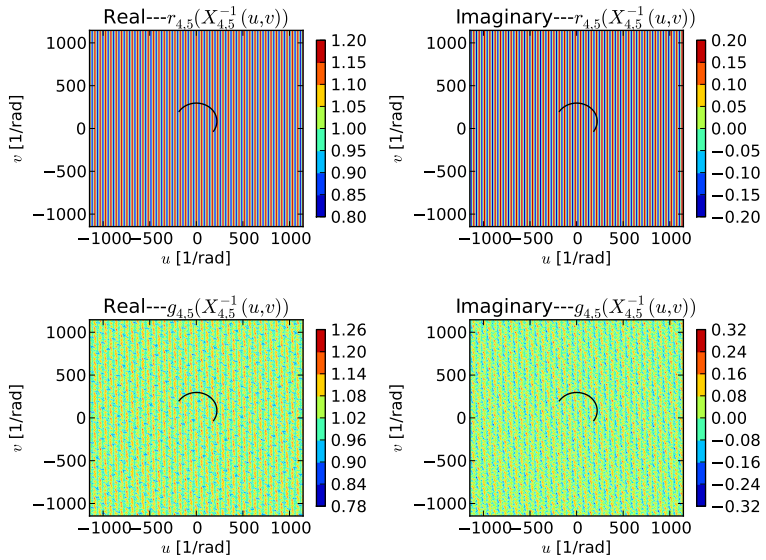

Figure 2: The extrapolated observed (top panel) and calibrated visibility (bottom panel) plains for KAT-7 antenna 4 and 5. The flux values of the two sources are equal to $A_1 = 1$ Jy and $A_2 = 0.2$ Jy and the position vector of the unmodelled source is $(1°, 0°)$. The black ellipitical locus, is the uv coverage associated with antenna 4 and 5.

Taking the inverse Fourier transform of $g_{4,5}(\hat{X}_{4,5}^{-1}(\boldsymbol{b}))$ produces the calibrated sky seen by the baseline associated with antenna 4 and 5. By taking the Fourier inverse of Eq. 11 we can determine the position vectors of the bright ghosts. The simulated (without extrapolation – staying on $\boldsymbol{b}_0$) and theoretical (using extrapolation) ghost pattern results can be obtained in Fig. 4 and Fig. 5. The theoretical and simulated results correspond well, validating Eq. 11.

4 Conclusion

We have shown that for a general array layout, ghosts no longer form in a straight line (connecting the modelled and unmodelled source). This paper is very brief and only deals with the artefacts contained in calibrated visibilities. An extension to the corrected visibility case will be discussed in a future work.

References

[1] Boonstra A.J. and van der Veen A.J., "Gain calibration methods for radio telescope arrays",*IEEE Transactions on Signal Processing*, vol. 51, no. 1, 2003, pp. 25–38.

[2] Grobler T.L., C.D. Nunhokee, O.M. Smirnov, A.J. van Zyl and A.G. de Bruyn, "Calibration artefacts in radio interferometry – I. Ghost sources in Westerbork Synthesis Radio Telescope data", *Montly Notices of the Royal Astronomical Society*, vol. 439, no. 4, 2014, pp. 4035–4047.

[3] Martí-Vidal I. and Marcaide J.M., "Spurious source generation in mapping from noisy phase-self-calibrated data", *Astronomy and Astrophysics*, 480, 2008, pp. 289–295.

[4] Smirnov O.M., "Revisiting the radio interferometer measurement equation. III. Addressing direction-dependent effects in 21 cm WSRT observations of 3C 147", *Astronomy and Astrophysics*, 527, A108, 2011.

[5] Thompson A.R., Moran J.M., and Swenson G.W., "Interferometry and synthesis in radio astronomy", John Wiley & Sons, 2008.

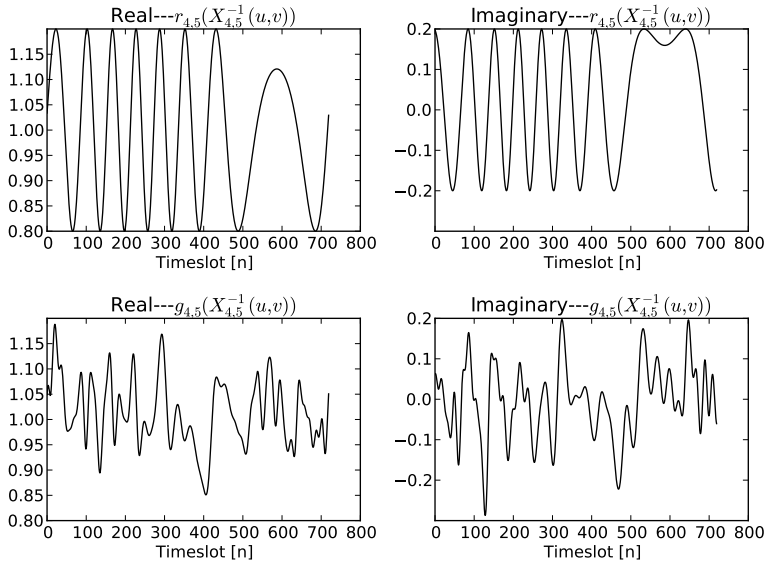

Figure 3: The visibilies that are recorded on the black elliptical track in Fig. 2. These are the only visibilities one would obtain without extrapolation.

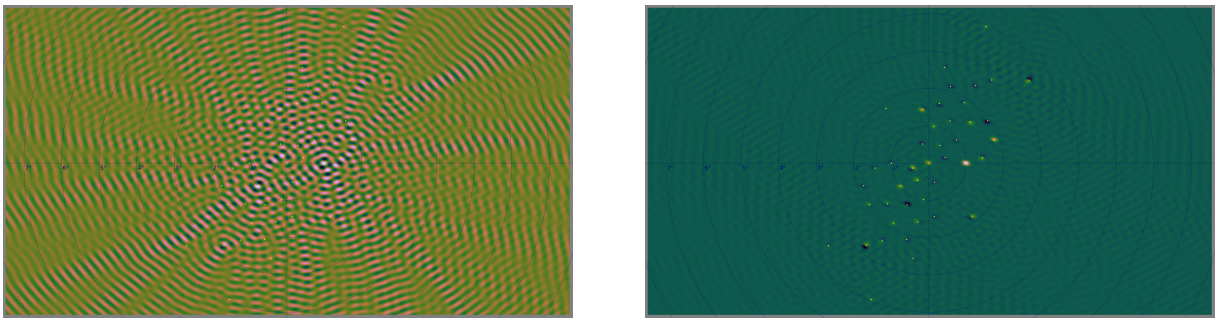

Figure 4: The dirty (right panel) and clean image (left panel) of the distilled calibrated sky (calculated via simulations – the Fourier inverse of the calibrated visibilities in Fig 3) seen by baseline 45 (i.e. $g_{4,5}(\hat{X}_{4,5}^{-1}(\boldsymbol{b}_{4,5}))-1$). The yellow markers are the theoretical ghost positions predicted by Eq. 11. The clean image was obtained using Hogbom CLEAN, with a loop gain of 0.1 and a threshold of 0.01mJy. Some of the sources do contain some CLEAN artefacts around them, which indicates that the threshold is to low. The low threshold was selected, so that the faint ghosts would at least be visible.

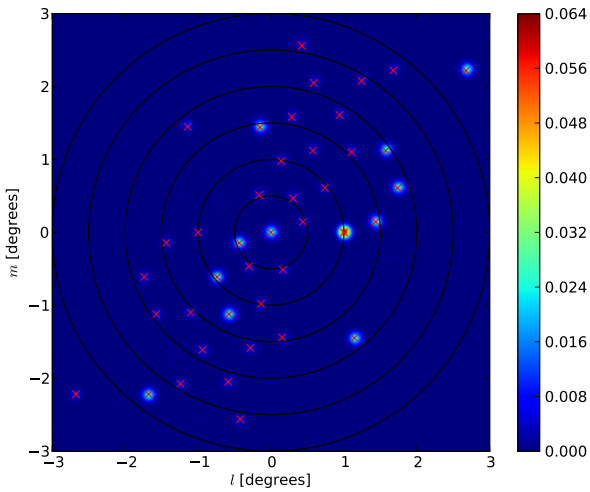

Figure 5: The absolute theoretical distilled calibrated sky $|\mathcal{F}^{-1}\{g_{4,5}(\hat{X}_{4,5}^{-1}(\boldsymbol{b}))-1\}|$ (derived by taking the inverse Fourier transform of the extrapolated calibrated visibility plain in Fig. 2). The red crosses are the predicted ghost positions predicted by Eq. 11.